Downloaded from orbit.dtu.dk on: May 06, 2023

DTU Library

Long-term strain response of polymer optical fiber FBG sensors

Bundalo, Ivan-Lazar; Nielsen, Kristian; Woyessa, Getinet; Bang, Ole

Published in:
Optical Materials Express

Link to article, DOI:
10.1364/OME.7.000967

Publication date:
2017

Document Version
Publisher's PDF, also known as Version of record

Link back to DTU Orbit

Citation (APA):
Bundalo, I-L., Nielsen, K., Woyessa, G., & Bang, O. (2017). Long-term strain response of polymer optical fiber FBG sensors. *Optical Materials Express*, *7*(3), 967-976. https://doi.org/10.1364/OME.7.000967

General rights
Copyright and moral rights for the publications made accessible in the public portal are retained by the authors and/or other copyright owners and it is a condition of accessing publications that users recognise and abide by the legal requirements associated with these rights.

- Users may download and print one copy of any publication from the public portal for the purpose of private study or research.
- You may not further distribute the material or use it for any profit-making activity or commercial gain
- You may freely distribute the URL identifying the publication in the public portal

If you believe that this document breaches copyright please contact us providing details, and we will remove access to the work immediately and investigate your claim.

Research Article | Vol. 7, No. 3 | 1 Mar 2017 | OPTICAL MATERIALS EXPRESS 967

Optical Materials EXPRESS

Long-term strain response of polymer optical fiber FBG sensors

IVAN-LAZAR BUNDALO,* KRISTIAN NIELSEN, GETINET WOYESSA, AND OLE BANG

DTU Fotonik, Technical University of Denmark, Ørsteds Plads B343, 2800 Kgs. Lyngby, Denmark
**ivlab@fotonik.dtu.dk*

Abstract: We report on the viscoelastic response of PMMA microstructured polymer optical fibers (mPOFs) when exposed to long periods of strain and relaxation, with the strain period ranging from 0.5 min to 50 min. The behavior of the fibers was monitored by inscribing a fiber Bragg grating (FBG) in them and tracking the reflection peak. We demonstrate that the fiber, when relaxing from strains of up to 0.9%, has a two-phase recovery: initially linear (elastic driven) and subsequently nonlinear (viscoelastic driven) contraction. The linear (elastic) relaxation wavelength range depends both on the strain level and on the strain duration. For short strain durations, this wavelength range stays the same, but with increasing strain duration, it decreases, which will influence the operation range of mPOF and POF-based FBG sensors.

© 2017 Optical Society of America

OCIS codes: (060.2270) Fiber characterization; (060.2370) Fiber optics sensors; (060.3735) Fiber Bragg gratings; (060.4005) Microstructured fibers; (160.5470) Polymers.

References and links

1. A. D. Kersey, M. Davis, H. J. Patrick, M. LeBlanc, K. P. Koo, C. G. Askins, M. Putnam, and E. J. Friebele, "Fiber grating sensors," J. Lightwave Technol. **15**(8), 1442–1463 (1997).
2. K. O. Hill and G. Meltz, "Fiber Bragg grating technology fundamentals and overview," J. Lightwave Technol. **15**(8), 1263–1276 (1997).
3. D. J. Webb, "Fibre Bragg grating sensors in polymer optical fibres," Meas. Sci. Technol. **26**(9), 092004 (2015).
4. A. Cusano, D. Paladino, A. Cutolo, A. Iadicicco, and S. Campopiano, *Fiber Bragg Grating Sensors: Recent Advancements, Industrial Applications and Market Exploitation* (Bentham Science Publishers, 2012).
5. A. Cusano, A. Cutolo, and J. Albert, *Fiber Bragg Grating Sensors: Recent Advancements, Industrial Applications and Market Exploitation* (Bentham Science, 2009).
6. M. Large, G. W. Barton, L. Poladian, and M. A. van Eijkelenborg, *Microstructured Polymer Optical Fibre*, 1st ed. (Springer, 2008).
7. A. Stefani, S. Andresen, W. Yuan, and O. Bang, "Dynamic characterization of polymer optical fibers," IEEE Sens. J. **12**(10), 3047–3053 (2012).
8. D. Sáez-Rodríguez, K. Nielsen, O. Bang, and D. J. Webb, "Time-dependent variation of fiber Bragg grating reflectivity in PMMA-based polymer optical fibers," Opt. Lett. **40**(7), 1476–1479 (2015).
9. A. Stefani, S. Andresen, W. Yuan, N. Herholdt-Rasmussen, and O. Bang, "High sensitivity polymer optical fiber-Bragg-grating-based accelerometer," Photonics Technol. Lett. IEEE **24**(9), 763–765 (2012).
10. G. D. Peng, Z. Xiong, and P. L. Chu, "Photosensitivity and gratings in dye-doped polymer optical fibers," Opt. Fiber Technol. **5**(2), 242–251 (1999).
11. H. Dobb, D. J. Webb, K. Kalli, A. Argyros, M. C. J. Large, and M. A. van Eijkelenborg, "Continuous wave ultraviolet light-induced fiber Bragg gratings in few- and single-mode microstructured polymer optical fibers," Opt. Lett. **30**(24), 3296–3298 (2005).
12. I.-L. Bundalo, K. Nielsen, C. Markos, and O. Bang, "Bragg grating writing in PMMA microstructured polymer optical fibers in less than 7 minutes," Opt. Express **22**(5), 5270–5276 (2014).
13. R. Oliveira, L. Bilro, and R. Nogueira, "Bragg gratings in a few mode microstructured polymer optical fiber in less than 30 seconds," Opt. Express **23**(8), 10181–10187 (2015).
14. J. Capodagli and R. Lakes, "Isothermal viscoelastic properties of PMMA and LDPE over 11 decades of frequency and time: A test of time-temperature superposition," Rheol. Acta **47**(7), 777–786 (2008).
15. K. Krebber, S. Liehr, and J. Witt, "Smart technical textiles based on fibre optic sensors," in *OFS2012 22nd International Conference on Optical Fiber Sensors, Invited Paper*, Y. Liao, W. Jin, D. D. Sampson, R. Yamauchi, Y. Chung, K. Nakamura, and Y. Rao, eds. (2012), Vol. 8421, p. 84212A–10.
16. W. Yuan, A. Stefani, and O. Bang, "Tunable polymer fiber Bragg grating (FBG) inscription: Fabrication of dual-FBG temperature compensated polymer optical fiber strain sensors," IEEE Photonics Technol. Lett. **24**(5), 401–403 (2012).

#279555 https://doi.org/10.1364/OME.7.000967
Journal © 2017 Received 26 Oct 2016; revised 13 Jan 2017; accepted 13 Jan 2017; published 21 Feb 2017

Optical Materials EXPRESS

17. I. P. Johnson, W. Yuan, A. Stefani, K. Nielsen, H. K. Rasmussen, L. Khan, D. J. Webb, K. Kalli, and O. Bang, "Optical fibre Bragg grating recorded in TOPAS cyclic olefin copolymer," Electron. Lett. **47**(4), 271 (2011).
18. G. Woyessa, A. Fasano, A. Stefani, C. Markos, K. Nielsen, H. K. Rasmussen, and O. Bang, "Single mode step-index polymer optical fiber for humidity insensitive high temperature fiber Bragg grating sensors," Opt. Express **24**(2), 1253–1260 (2016).
19. C. Markos, A. Stefani, K. Nielsen, H. K. Rasmussen, W. Yuan, and O. Bang, "High-Tg TOPAS microstructured polymer optical fiber for fiber Bragg grating strain sensing at 110 degrees," Opt. Express **21**(4), 4758–4765 (2013).
20. A. Fasano, G. Woyessa, P. Stajanca, C. Markos, A. Stefani, K. Nielsen, H. K. Rasmussen, K. Krebber, and O. Bang, "Fabrication and characterization of polycarbonate microstructured polymer optical fibers for high-temperature-resistant fiber Bragg grating strain sensors," Opt. Mater. Express **6**(2), 649 (2016).
21. A. Lacraz, M. Polis, A. Theodosiou, C. Koutsides, and K. Kalli, "Femtosecond Laser Inscribed Bragg Gratings in Low Loss CYTOP Polymer Optical Fiber," IEEE Photonics Technol. Lett. **27**(7), 693–696 (2015).
22. Z. Xiong, G. D. Peng, B. Wu, and P. L. Chu, "Highly tunable Bragg gratings in single-mode polymer optical fibers," IEEE Photonics Technol. Lett. **11**(3), 352–354 (1999).
23. B. T. Kuhlmey, R. C. McPhedran, and C. Martijn de Sterke, "Modal cutoff in microstructured optical fibers," Opt. Lett. **27**(19), 1684–1686 (2002).
24. A. Stefani, K. Nielsen, H. K. Rasmussen, and O. Bang, "Cleaving of TOPAS and PMMA microstructured polymer optical fibers: Core-shift and statistical quality optimization," Opt. Commun. **285**(7), 1825–1833 (2012).
25. D. X. Yang, J. Yu, X. Tao, and H. Tam, "Structural and mechanical properties of polymeric optical fiber," Mater. Sci. Eng. A **364**(1–2), 256–259 (2004).
26. W. Zhang and D. J. Webb, "Humidity responsivity of poly (methyl methacrylate) - based optical fiber Bragg grating sensors," Opt. Lett. **39**(10), 3026–3029 (2014).
27. W. Yuan, L. Khan, D. J. Webb, K. Kalli, H. K. Rasmussen, A. Stefani, and O. Bang, "Humidity insensitive TOPAS polymer fiber Bragg grating sensor," Opt. Express **19**(20), 19731–19739 (2011).
28. H. F. Brinson and L. C. Brinson, *Polymer Engineering Science and Viscoelasticity* (Springer US, 2015).
29. A. Abang and D. J. Webb, "Influence of mounting on the hysteresis of polymer fiber Bragg grating strain sensors," Opt. Lett. **38**(9), 1376–1378 (2013).

1. Introduction

A common method for sensing with optical fibers is through Fiber Bragg Gratings (FBGs). FBGs in silica fibers have been used for decades [1,2], finding applications in structural health monitoring, in high temperature environments, and in environments with strong electro-magnetic fields, where all metal components are unwanted or would not function. However, silica fibers have some limitations, such as a large Young's modulus and limited biological compatibility due to danger of glass debris [3,4]. The solutions to these limitations might be found in polymer optical fibers (POFs). Polymer is a suitable material for a number of sensing applications unreachable for silica because polymer has a higher elastic limit and lower Young's modulus [3–6]. However, unlike silica fibers, POFs are still missing substantial information regarding their long term mechanical properties. In particular, due to their viscoelastic nature, POFs have a nonlinear response when strained and relaxed [7,8]. While POFs have high transmission losses in comparison to silica, this does not pose a considerable drawback in certain applications requiring only short sensor fiber lengths, such as accelerometers or microphones [9]. FBGs are most commonly inscribed into the fiber through the phase mask technique using a CW [10–12] or pulsed laser [13], and a common method for monitoring the response is through tracking the peak reflection wavelength.

The viscoelasticity of polymers mean that their mechanical properties can vary significantly depending on the duration and frequency of the applied strain [14]. The majority of instruments used to measure viscoelastic properties of materials are only capable of testing a limited range of loading frequencies so, although polymer viscoelasticity was broadly studied for bulk materials, the viscoelastic behavior of POFs is still expected to hold somewhat unique properties due to the elongated shape and drawing conditions.

In applications, such as geogrids, smart textiles, and endoscopic manometers, POF-based sensors would be experiencing different levels of strain for various durations of time [15]. Fiber relaxation or recovery, as it is commonly known in mechanics, is of great interest for commercialization of POF sensors, in particular it is important to find the limits of viscoelasticity under different levels and durations of strain. The frequency regime of up to 10

Optical Materials EXPRESS

kHz, which could be used for acoustic and vibration sensing, has already been investigated by Stefani et al. [9]. The quasi-static behavior of UV-written polymer FBGs under strain and relaxation was also recently investigated [8,16]. Here we study the behavior of POF FBGs in the low-frequency regime (between high frequency [9] and quasi-static behavior [8,16]), where the period of straining and relaxation takes place on time scales larger than 1 second. It should be noted that in this manuscript relaxation does not mean stress relaxation, but fiber relaxation, i.e., fiber contraction after it is no longer under external strain. While FBGs have been inscribed into several types of POFs and mPOFs, such as TOPAS [17,18], High-Tg TOPAS [19], polycarbonate [20], and CYTOP [21], we here limit ourselves to the most commonly used PMMA POF, in which the first POF [22]and mPOF [11] FBGs were reported in 1990 and 2005, respectively.

2. The experiment

The fiber used for the investigation was fabricated in-house using a POF draw tower and is made of Polymethyl methacrylate (PMMA). The fiber has a cladding with a hexagonal 3-ring photonic crystal structure, with a pitch (hole-to-hole distance) of 3.75 µm and a hole-to-pitch ratio of 0.26, making it endlessly single-mode [23]. The fiber outer diameter was 130 µm. An FBG was inscribed into the fiber using the phase mask technique [12]. After annealing the fiber for 48h at 85°C, the relaxed FBG peak wavelength was at 618.7 nm. A silica fiber was used to launch light into the POF and collect the reflected response of the FBG. The PMMA POF was prepared by cleaving at an optimal temperature of around 77°C [24] of both the blade and POF to ensure optimal coupling to the silica fiber. The response was monitored using a supercontinuum light source (SuperK Power from NKT Photonics) and the light was analyzed using an OceanOptics HR2000 spectrometer. The Fiber had an initial length of 14 cm and was strained to a maximum of 0.9% to stay well clear of too high strains that might induce material deformation [25].

The fiber was mounted between a fixed and a motorized linear translation stage (see Fig. 1 left). The motorized stage was used to apply the targeted strain for a certain duration. In Fig. 1 (right) the blue curve shows the movement of the motor, which takes less than half a second to apply the strain. The purple dotted curve shows the reflected signal from the FBG; on the upstroke it follows rapidly the movement of the motor, but on the downstroke it has a time-lag in its response. This unwanted time-lag appears due to the viscoelastic nature of polymer, and is the subject of this investigation.

The experiment was performed in an environment with a controlled temperature and humidity, where the change of temperature was less than 2°C and the humidity (RH) change was less than 2% in each sequence of experiment. This is important due to the temperature and humidity response of POFs [26,27].

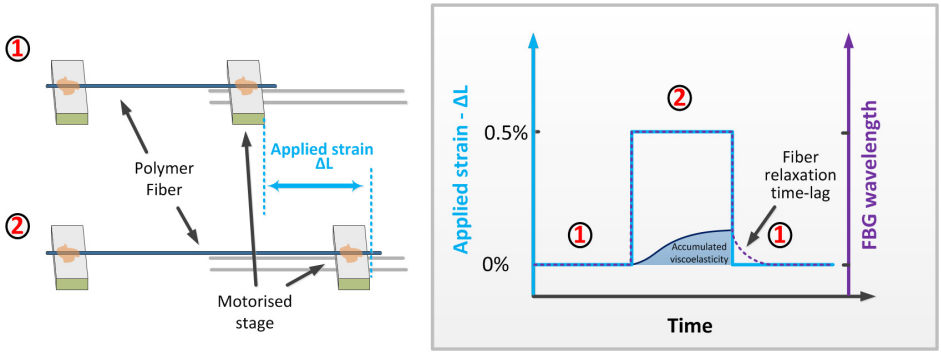

Fig. 1. Experimental setup - the fiber has been strained with the help of a motorized stage (left). The fiber relaxation (recovery) was monitored through the reflected FBG peak. While the motorized stage moved consistently, due to the viscoelastic nature of polymer, the FBG peak had a time lag in relaxing to the initial position (right).

Optical Materials EXPRESS

2.1 Strain of 0.4%

The fiber was initially stretched by 0.7 mm, which corresponds to 0.4% strain. The fiber was kept strained for a time T_1 (initially 0.5 minutes), and subsequently released to recover for a time T_2 (always 5 minutes). The time lag of the fiber recovery was visible in the bottom part of the relaxation curve.

The fiber relaxation can be divided into two relaxation ranges in terms of the wavelength: the fast linear elastic relaxation range $\Delta\lambda_{FAST}$, followed by the slow nonlinear viscous-dominated relaxation range $\Delta\lambda_{SLOW}$. $\Delta\lambda_{FAST}$ is defined as the range where the fiber is following the (rapidly decreasing) strain applied by the motor. $\Delta\lambda_{SLOW}$ is defined as the range in which the fiber has a time-lag when relaxing, and does not follow the (rapidly decreasing) strain anymore; it is defined to start when the rate of the FBG peak shift has decreased by a factor of 20. To see the evolution of the time lag and the hysteresis it produces, we repeated the same strain cycle 10 times. The scheme explaining the procedure is shown in Fig. 2, with $\Delta\lambda_{FAST}$ and $\Delta\lambda_{SLOW}$ ranges indicated in the right side of the figure.

The 10-cycle sequence was repeated 4 times with different values of the strain time T_1 (2.5, 5, 10 and 50 minutes), with the fiber relaxation time T_2 kept constant at 5 minutes. After each sequence the fiber was left relaxing for 2 hours to mitigate any possible accumulated stress before the new sequence took place.

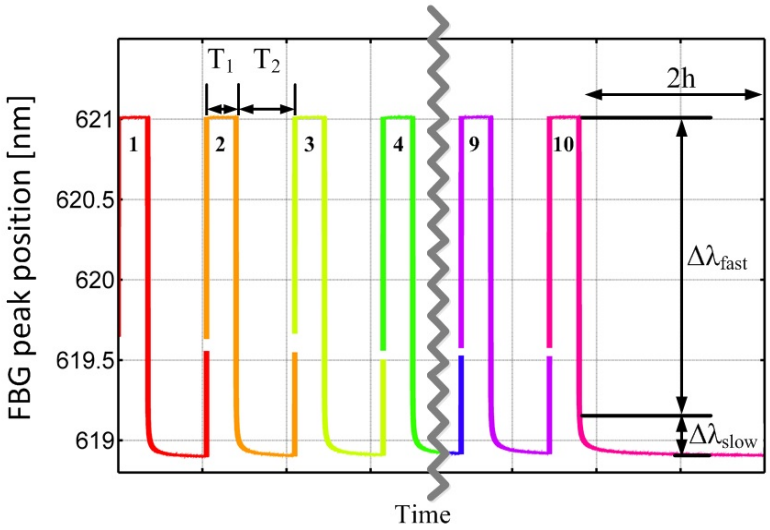

Fig. 2. Schematic of a sequence of the experiment. The fiber is strained (here 0.4%) for the duration T_1 and then relaxed for the duration T_2. After a sequence of 10 repetitions of the strain-relax cycle, the fiber was left relaxing (recovering) for two hours to mitigate possible accumulated stress. The two main relaxation ranges are indicated in the right side of the figure: the linear (elastic-driven) fast relaxation range $\Delta\lambda_{FAST}$, followed by the nonlinear (viscous-dominated) slow relaxation range $\Delta\lambda_{SLOW}$. $\Delta\lambda_{FAST}$ is defined as the range where the fiber is following the (rapidly decreasing) strain applied by the motor. $\Delta\lambda_{SLOW}$ is defined as the range in which the fiber has a time-lag and does not follow the (rapidly decreasing) strain anymore; defined as when the speed of the FBG peak shift has become 20 times slower than the motor speed.

In Fig. 3, each of the 5 windows represent a different value of the strain time T_1. Each window contains 10 curves for 10 cycles (a sequence as shown in Fig. 2.) overlaid one over another.

Optical Materials EXPRESS

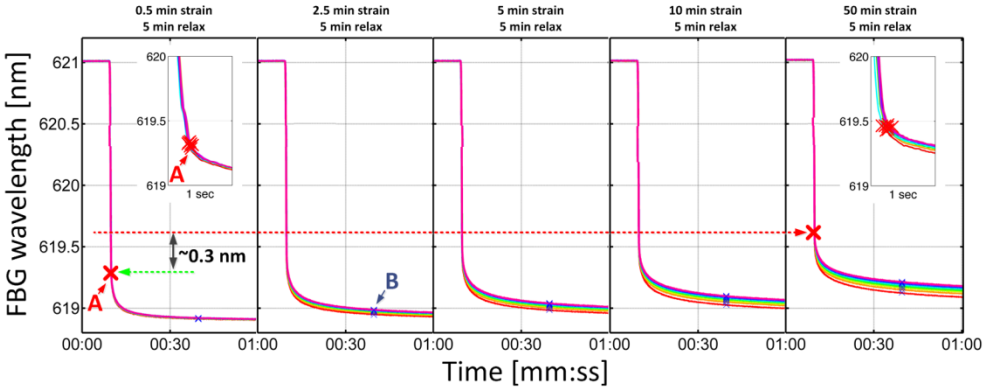

Fig. 3. Strain-relaxation sequences for a strain level of 0.4%. Each window shows a sequence of 10 overlaid cycles as presented in Fig. 2. The strain time T_1 in the five windows is 0.5, 2.5, 5, 10, and 50 min, respectively, while the relaxation time T_2 was kept constant at 5 min. The point A (red X) marks the boundary between $\Delta\lambda_{FAST}$ and $\Delta\lambda_{SLOW}$, with the inset image showing it more precisely. The point B (blue X) marks the point 30 seconds after the start of the relaxation. It is apparent that with increasing strain duration, the fiber takes longer time to relax. The linear range $\Delta\lambda_{FAST}$ is decreased by 0.3 nm when the strain duration is increased from 0.5 min (dashed green arrow) to 5 min (dashed red arrow), thereby reducing the $\Delta\lambda_{FAST}$ range by about 18%.

For short strain times T_1 = 0.5 min, presented in the leftmost window of Fig. 3, a relaxation time of 5 minutes is enough for a nearly complete relaxation of the fiber to where the FBG has the fully relaxed center wavelength 618.7 nm. During the sequence no hysteresis is visible, all 10 curves seem to perfectly overlap one over another. With increasing strain time T_1, the fiber requires longer time to relax (due to the memory effect of accumulated stress [28]), and the 5 min relaxation time is no longer enough to sufficiently relax the fiber; as a result hysteresis starts appearing.

Looking at the most extreme case of T_1 = 50 min, the rightmost window in Fig. 3, we find that $\Delta\lambda_{SLOW}$ reaches the value of 0.8 nm. The whole strain range is ≈2.3 nm, so $\Delta\lambda_{SLOW}$ takes up as much as 35% of the whole strain range. That means that in sensing applications a free POF FBG sensor would not be able to monitor the strain in real-time during the last 35% of the relaxation. However, applying a sufficient prestrain found by monitoring $\Delta\lambda_{SLOW}$, the sensor could function in real time, which is the key subject of our further investigations.

2.2 Strain of 0.9%

The whole experiment was repeated with a strain of 0.65% and 0.9%, but for convenience of explanation we are presenting only the data for 0.9% strain, for which the strained FBG has an average peak wavelength of 623.85 nm. In the leftmost window of Fig. 4 it is observable that for 0.9% strain there is a small degree of hysteresis (the point B increases) even for the shortest strain time T_1 = 0.5 min, as the fiber does not manage to relax to the initial 618.7 nm within 5 mins, but stays above 619 nm. The hysteresis becomes more apparent and pronounced with increasing strain duration. For 0.9% strain $\Delta\lambda_{FAST}$ is more than twice that for 0.4% strain. For the short strain time of T_1 = 0.5 min $\Delta\lambda_{FAST}$ ≈1.8 nm for 0.4% strain, while for 0.9% strain it is $\Delta\lambda_{FAST}$ ≈3.8 nm. For the longest strain time T_1 = 50 min we find $\Delta\lambda_{FAST}$ ≈1.5 nm for 0.4% strain, while for 0.9% strain $\Delta\lambda_{FAST}$ ≈4.2 nm.

Optical Materials EXPRESS

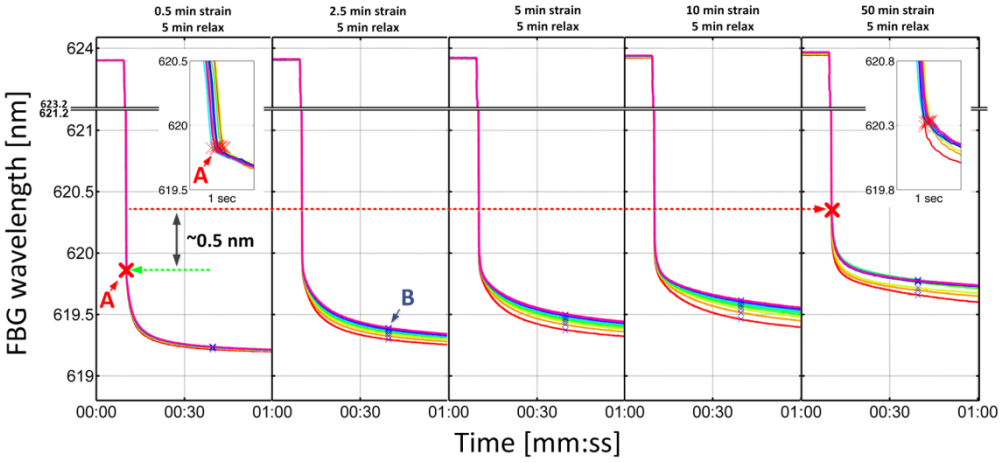

Fig. 4. 10 cycle strain-relaxation sequence for a strain of 0.9% and different durations of strain T_1 (same marking as in Fig. 3). The wavelength range $\Delta\lambda_{FAST}$ is decreased by 0.5 nm when the strain duration is increased from 0.5 min (dashed green arrow) to 50 min (red arrow), thereby reducing the wavelength range of fast contraction $\Delta\lambda_{FAST}$ by about 13%.

A small increase in the fully strained FBG wavelength (top flat level) is visible as the fiber is strained more and more in Figs. 3. and 4, most pronounced in Fig. 4 with 0.9% strain. In fact, the FBG wavelength increases slightly also during each individual strain period, despite the motor holding the same position. This is demonstrated for cycle 1 and 10 for all strain times in Fig. 5. It means that this effect is not due to temperature. Furthermore, it rises more for longer strain times than for shorter. The acrylic glue used to glue the fiber to the motorized stage is more rigid than the fibers, so this slight rise could be partially due to the glue.

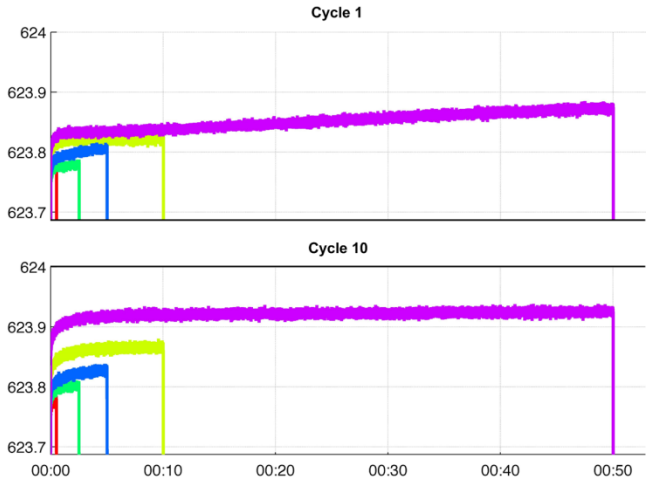

Fig. 5. FBG growth during the straining time for cycle 1 and 10 for all the different strain times.

We believe that this increase is mainly due to internal rearrangement of the polymer chains, which release the tension in the fiber and, through it, influence the FBG wavelength. Further studies would be needed to thoroughly investigate this behavior. Since the effect leads to a change on the order of only 0.1nm we here neglect it and focus on the relaxation dynamics.

Optical Materials EXPRESS

3. Hysteresis evolution

To observe the change in the relaxation hysteresis, the fiber was examined 30 seconds after the start of relaxation, marked with a blue X and labeled B in Figs. 3-4. This point is easy to track automatically and is well into the viscous part of the relaxation in all cases in Figs. 3-4. Thus, a significant change in the FBG wavelength at point B should be visible when changing the strain time T_1. The evolution of the FBG center wavelength at position B with the number of strain cycles is shown in Fig. 6 for different strain times T_1. It is apparent for both 0.4% strain [Fig. 6(a)] and 0.9% strain [Fig. 6(b)] that for the shortest strain time T_1 = 0.5 min (red curves) the fiber can follow the strain cycle with almost no hysteresis, i.e., the FBG center wavelength after each cycle is almost constant.

When increasing the strain duration T_1 (orange, yellow, green, and turquois lines), the accumulated stress influences the subsequent cycles because the fiber cannot fully relax within the fixed relaxation time of T_2 = 5 min. As a consequence hysteresis starts appearing, i.e., the wavelength at point B increases with the number of strain cycles. However, importantly the wavelength at point B is seen to saturate towards an equilibrium, at which hysteresis has again disappeared. For the longest strain durations T_1, the equilibrium has not been reached after 10 cycles and thus hysteresis is still present. For shorter T_1, it appears that the fiber comes close to an equilibrium at which hysteresis is no longer present.

When comparing 0.4% and 0.9% strain, perhaps the most apparent observation is the big offset in the FBG positions measured at point B. They are different by at least 0.3 nm, which corresponds to about 0.9% strain. The wavelength at the B points is higher for 0.9% strain than for 0.4%, but the FBGs strained for 0.9% still have an overall much bigger fast relaxation range $\Delta\lambda_{FAST}$ due to the larger total strain.

The main reason that the light green curve for T_2 = 50 minutes in Fig. 6(b), is not as smooth as the other curves is due to a drift in the otherwise humidity and temperature controlled environment.

We would now like to investigate the viscoelastic response of the mPOF FBG and in particular follow how the fast and slow response regimes $\Delta\lambda_{FAST}$ and $\Delta\lambda_{SLOW}$ vary with the strain time T_1. It would be highly important for applications if the disappearance of the hysteresis after a certain number of strain cycles observed in Fig. 6 translates into an upper limit of the slow viscous regime $\Delta\lambda_{SLOW}$. This would mean that the mPOF FBG sensor could be characterized by a constant available fast relaxation range independent of the number of strain cycles. By proper prestraining, the sensor could then be made to follow the applied strain perfectly.

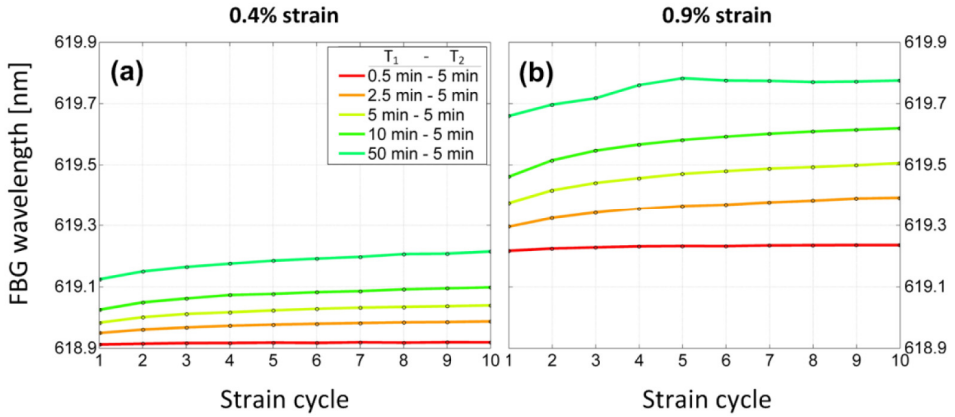

Fig. 6. Center FBG wavelength at point B, which is 30 seconds after the start of relaxation (see marks in Figs. 3- 4), versus the number of strain cycles in a 10-cycle sequence. The sequences with 0.4% strain are shown in (a), while the sequences with 0.9% strain are shown in (b). For each strain level we show 5 sequences with varying strain time T_1.

Optical Materials EXPRESS

To follow $\Delta\lambda_{FAST}$ and $\Delta\lambda_{SLOW}$ we have manually evaluated the wavelength level separating the two regimes, which is marked as the red point A in Figs. 3 and 4. In Fig. 7 we plot this wavelength versus the strain time T_1, both when measured in the first strain cycle (blue curves) and in the last 10th strain cycle (red curves). In addition to 0.4% and 0.9% strain, we also plotted the data for 0.65% strain. The results are showing that with increasing strain time T_1, the wavelength at point A (and therefore $\Delta\lambda_{SLOW}$) increases but eventually reaches an equilibrium. This indicates that, at least for these strain levels, there will always be a considerable amount of $\Delta\lambda_{FAST}$ even if the strain durations are longer than 50 min.

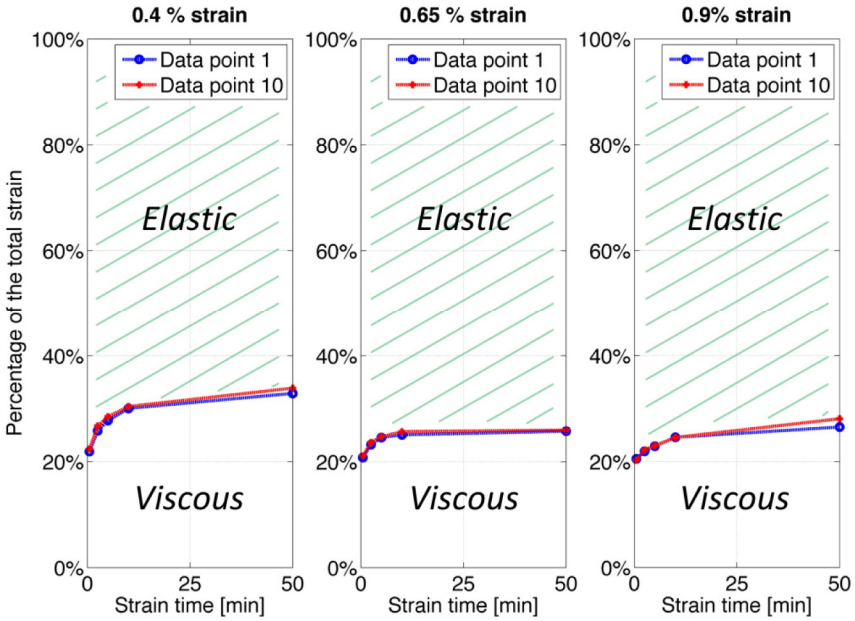

Fig. 7. Wavelength at point A versus strain time T_1, for 0.4% strain (left), 0.65% strain (center) and 0.9% strain (right). The Y-axis is scaled to percentage of total strain for direct comparison. For both the first and the last, 10th, iteration (red and blue curves, respectively), after 50 mins $\Delta\lambda_{FAST}$ shrank to about 70% of the total strain, for each of the different strain levels. The values for the 10th strain cycle differ by less than 3% (of the total strain range) from the values for the first iteration.

Table 1. Summary of $\Delta\lambda_{FAST}$ and $\Delta\lambda_{SLOW}$ for 0.4%, 0.65% and 0.9% strain for shortest and longest strain duration T_1. The values are taken for the 10th cycle (red curves presented in Fig. 6). The brackets give the percentage of the total strain that the particular wavelength range corresponds to.

	T_1 = 0.5 min $\Delta\lambda_{FAST}$	T_1 = 0.5 min $\Delta\lambda_{SLOW}$	T_1 = 50 min $\Delta\lambda_{FAST}$	T_1 = 50 min $\Delta\lambda_{SLOW}$
0.4% strain	1.8 nm (78%)	0.5 nm (22%)	1.5 nm (65%)	0.80 nm (35%)
0.65% strain	3.1 nm (79%)	0.8 nm (21%)	2.9 nm (74%)	1 nm (26%)
0.9% strain	4.2 nm (79%)	1.1 nm (21%)	3.8 nm (73%)	1.4 nm (27%)

The main conclusion from Fig. 7 and Table 1 is that for the strain times and strain levels tested here, the desired fast relaxation range $\Delta\lambda_{FAST}$ always covers more than 65% of the whole strain range. One should keep in mind that these values are valid for unembedded sensors and that the relaxation will be dependent on the host material if the sensor is embedded [29]. It should be noted that after the experiments were conducted, the fiber took about a week to relax completely to have the FBG center wavelength at the initial unstrained value 618.7 nm.

Optical Materials EXPRESS

4. Operational range for FBG sensors

Our results have shown that the viscous range of the sensor, $\Delta\lambda_{SLOW}$, stays below 35% of the total wavelength shift due to the strain, for all the covered strain levels and strain and relaxation times. The apparent saturation in the growth of the undesired slow viscous response $\Delta\lambda_{SLOW}$ is important. It implies that if the mPOF FBG sensor is pre-strained to shift the FBG wavelength sufficiently more than the upper limit of $\Delta\lambda_{SLOW}$ then the response of the sensor would always be in the instantaneous $\Delta\lambda_{FAST}$ regime.

To confirm this, an additional test has been made. A new fiber has been strained for 1 hour at 1% strain (FBG wavelength going from 602.1 nm to 607.9 nm) and after that relaxed to determine the point A (the beginning of $\Delta\lambda_{SLOW}$ shown in Figs. 3 and 4.). The value of point A was determined to be at 603.7 nm, which gives a $\Delta\lambda_{SLOW}$ about 28% of the total strain range, which is somewhat lower than expect for 1h strain at 1% according to Fig. 8. and Table 1. However, one should remember that this is a new fiber from the same fiber spool, but with a new FBG.

For a proof-of-principle experiment we then pre-strained the fiber with 0.6% strain (FBG wavelength at 605.6 nm) to be absolutely certain to have no visible effects of the viscous regime $\Delta\lambda_{SLOW}$. To push the limit we performed 10 strain cycles with the sensor, in which the fiber was strained to 1% and relaxed to about 0.6%.

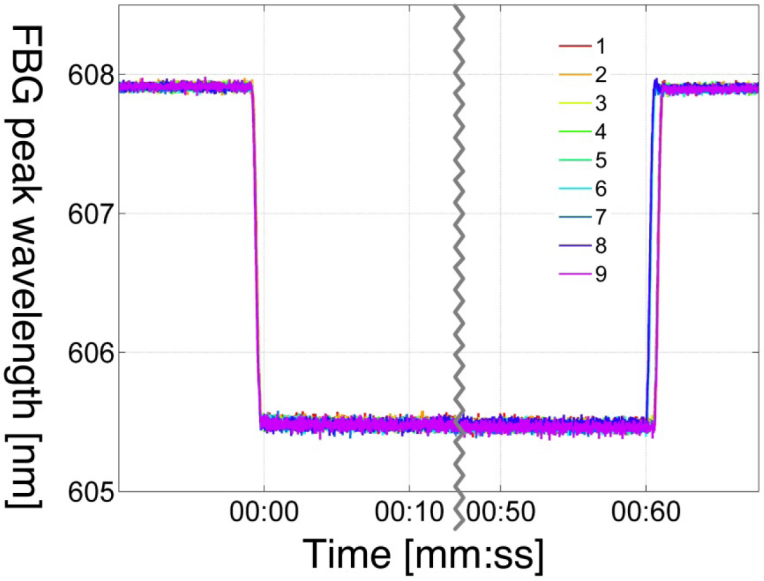

Fig. 8. A sequence of 10 strain-relax cycles where strain amounted to 1% and relax to 0.6%. The relaxation range $\Delta\lambda_{FAST}$ has been determined after straining the fiber for 1h at 1% and then completely relaxing to find the point A which was standing at 0.28% of the total strain. Afterwards, the fiber has been strained to 1% and relaxed to 0.6%, a value which was selected as it is sufficiently above measured point A. It appears that the FBG peak is following the motor movement very precisely without any time lag in response. A difference in the start of the rise for certain curves originates in counting error of the software running the strain motor, which sometimes adds a second on the 60 seconds count.

The 10 overlaid cycles are shown in Fig. 8 and as expected the FBG peak is indeed seen to follow the rapid motor movement very precisely without any time lag. On the upstrokes seen in the Fig. 8, there is sometimes a slight time-offset due to software counting error.

These results suggest that even for longer strain times than the ones tested here, we can tailor our sensor for the optimum operation by prestraining it above $\Delta\lambda_{SLOW}$. For longer

Optical Materials EXPRESS

strains, it would be necessary to first find $\Delta\lambda_{SLOW}$ and then operate the sensor at 10% or more above it.

5. Conclusion

POF-based FBG sensors have several advantages of their silica fiber counterpart, such as a lower Young's modulus and a higher breaking strain, which makes them particularly suitable for high-sensitivity sensing of even very large strains. However, the well-known viscous response of POF FBGs could be a potential problem. Here we have performed long-term quasi-static measurements of the response of POF FBGs for strain levels up to 0.9% and strain times of up to 50 minutes. We have tracked the slow viscous wavelength regime $\Delta\lambda_{SLOW}$ for 10 repeated cycles of strain and relaxation and found that, very importantly, any appearing hysteresis disappears after a sufficient number of strain relaxation cycles. Thus $\Delta\lambda_{SLOW}$ saturates and the fast relaxation range $\Delta\lambda_{FAST}$, during which the sensor can rapidly follow the strain, remains above 65% of the total wavelength interval. We have confirmed that this means that if a POF FBG sensor is sufficiently pre-strained, then it can always follow the applied strains we have investigated here in real time. Prestraining naturally limits the vailable sensing range, but in most applications the POF FBG would be embedded in more rigid host materials and thus prestraining would not be an issue.

130.225.94.43 {ts '2017-03-24 11:54:31'}